Feature preserving variational smoothing of terrain data

Tolga Tasdizen

School of Computing
University of Utah
Salt Lake City, UT 84112
e-mail: tolga@sci.utah.edu

Ross Whitaker

School of Computing
University of Utah
Salt Lake City, UT 84112
e-mail: whitaker@cs.utah.edu

Abstract

In this paper, we present a novel two-step, variational and feature preserving smoothing method for terrain data. The first step computes the field of 3D normal vectors from the height map and smoothes them by minimizing a robust penalty function of curvature. This penalty function favors piecewise planar surfaces; therefore, it is better suited for processing terrain data then previous methods which operate on intensity images. We formulate the total curvature of a height map as a function of its normals. Then, the gradient descent minimization is implemented with a second-order partial differential equation (PDE) on the field of normals. For the second step, we define another penalty function that measures the mismatch between the the 3D normals of a height map model and the field of smoothed normals from the first step. Then, starting with the original height map as the initialization, we fit a non-parametric terrain model to the smoothed normals minimizing this penalty function. This gradient descent minimization is also implemented with a second-order PDE. We demonstrate the effectiveness of our approach with a ridge/gully detection application.

1 Introduction

Terrain data contains information that is pertinent to a variety of applications. For instance, scientists estimate slope gradient and aspect for analysis of hydrological flow over terrain. These estimates are later used in flood path predictions for safety planning. Another application could be the analysis of the terrain of other planets to plan a route that will be taken by an unmanned, exploration vehicle. However, the level automation in this analysis is currently low and therefore, these are mostly time consuming, manual tasks. Standard image processing techniques are not optimal when applied to terrain data. Therefore, the first step in a push towards more automated analysis should be the development of processing techniques specific to terrain data.

Terrains are often represented as a collection of height measurements, i.e. a *digital elevation model* (DEM). Elevation values can be represented as points, contour lines or triangulated irregular networks. In this paper, we are interested in terrain data that is represented on a 2D regular, rectilinear grid, i.e. a height image. Such DEMs are usually created by stereo photogrammetry from aerial photographs, field surveys, or most commonly by manually digitizing contour maps.

DEMs are available in many different forms that vary in accuracy, and horizontal and vertical resolution. The highest resolution DEMs distributed by the United States Geological Survey (USGS) correspond to 7.5 minute quadrangle maps (1:24000 scale) with horizontal resolution of 10 or 30 meters [20]. Vertical accuracy of these DEMs varies with the desired mean error of 7 meters, but it is not unusual to have errors of up to 15 meters. The 7.5-Minute DEMs are created by optically scanning contour maps and then fitting an approximating surface. Errors can be produced when elevations are interpolated from digitized contours. There are many potential sources of errors that effect accuracy and uncertainty of terrain feature analysis using DEM data [21].

Some of the necessary tools for analysis of terrain data are ridge detection, segmentation and compression. All of these tools require that we are able to extract features of the terrain such as ridges and gullies in the presence of noise. In image processing, Perona & Malik (P&M) introduced an anisotropic diffusion process that can preserve edges between distinct regions while smoothing the noise within the regions [12]. Unfortunately, a direct application of this method to height maps yields unsatisfactory results, see Section 3. In this paper, we formulate a correct generalization of this method to height maps by posing it as an energy minimization problem on curvature. The variational method we propose is also geometric, i.e. it is independent of the parameterization.

The rest of this paper is organized as follows. Section 2 presents a brief overview of related work in the literature. Section 3 discusses edge preserving smoothing methods in image processing. Section 4 formulates a robust curvature energy for $2\frac{1}{2}$D height surfaces. Section 5 introduces our splitting strategy that gives an efficient and stable minimization procedure for this energy. Section 6 illustrates results of the proposed approach and demonstrates its advantages with in the context of a ridge/gully detection application. Section 7 summarizes the contributions of this paper.

2 Related Work

Perona & Malik introduced the anisotropic diffusion PDE for intensity images in their pioneering work [12]. Nordstrom [11] and Black *et al.* [1] have shown that P&M's diffusion is the gradient descent process for a robust energy function. Other researchers have proposed different energy metrics, such as total variation, which yield variations of the anisotropic diffusion PDE [14]. These approaches are all second-order PDEs. Tumblin and Turk propose a fourth-order PDE as a detail preserving contrast reduction method for depicting high contrast images on low contrast display devices [19]. Their LCIS (low curvature image simplifier) algorithm is related to the robust curvature minimization strategy proposed in this paper. However, their approach is for 2D images, whereas, we take into account the geometry of $2\frac{1}{2}$D height surfaces. Furthermore, we provide a variational generalization of anisotropic diffusion to such surfaces.

A problem related to ours is the smoothing of 3D surfaces. In the context of level set representations, mean curvature flow (MCF), a geometric PDE that minimizes surface area has been a popular choice for enforcing smoothness of the model [9, 24]. MCF is not a feature preserving process. Furthermore, it suffers from several problems including volume shrinkage, pinching of thin structures. In the computer graphics literature, smoothing surface meshes has been approached as an energy minimization problem [10, 8, 22] and as a filtering problem [17, 4, 7]. More recently, anisotropic diffusion processes have been proposed for surface meshes and level sets [3, 13, 16]. None of these methods make use of the specific properties of $2\frac{1}{2}$D height surfaces.

Depth reconstruction has been a major focus in earlier computer vision research [6, 18, 2]. More recently, in the context of height maps, a $2\frac{1}{2}D$ version of MCF has been derived [23]. Desbrun *et al.* propose a feature preserving denoising process for height maps [5]. Their approach is to use a second-order flow that is a modification of MCF that does not take into account the geometry of height maps.

3 Edge preserving smoothing for intensity images

An established solution to the smoothing problem is to pose it as the gradient descent of an energy function, and to implement the gradient descent as a non-linear partial differential equation (PDE). The choice of the energy function depends on the application, and it determines what part of the input signal is preserved and what part is eliminated as a result of the gradient descent PDE. In image processing , it is typical to use an energy that favors smoothness. For instance, the heat equation implements the gradient descent for the minimization of the integral of a quadratic penalty on the image gradient magnitude

$$\min_I \int_U \| \nabla I \|^2 \, dx \, dy \Longrightarrow \frac{dI}{dt} = \nabla \cdot \nabla I, \qquad (1)$$

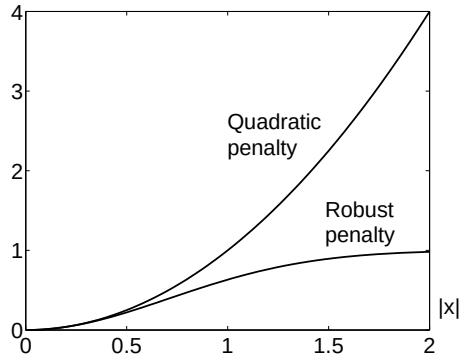

Figure 1: Comparison of quadratic and robust penalty functions.

where U is the domain of the image. Processing an image with the heat equation is mathematically equivalent to convolving it with a Gaussian smoothing kernel. It is a well known fact that such smoothing blurs boundaries in the image, and will go to a constant intensity level in the limit. This result is also expected from the variational point of view, because the quadratic penalty function, see Figure 1(a), does not permit the presence of high gradient magnitude outliers (edges). Figure 2(a) illustrates a surface described by a part of the Mt.Hood DEM. Figure 2(b) illustrates the results of treating this data as an intensity image and smoothing it with a Gaussian kernel. The ridges in the original data are rounded and distorted.

In their seminal work, Perona & Malik (P&M) introduced a non-linear, anisotropic diffusion PDE that can preserve edges while smoothing noise [12]. This method has gained popularity as a successful edge detection method in image processing. Nordstrom [11] and Black *et al.* [1] show that P&M anisotropic diffusion PDE is the gradient descent for a robust energy function:

$$\min_I \int_U 1 - e^{-\frac{\|\nabla I\|^2}{\mu^2}} \, dx \, dy \Longrightarrow \frac{dI}{dt} = \nabla \cdot \left(e^{-\frac{\|\nabla I\|^2}{\mu^2}} \nabla I \right). \qquad (2)$$

This robust penalty function, see Figure 1(b), is bounded for high values of its argument; therefore, it allows the presence of a limited number of outliers. Indeed, the P&M anisotropic diffusion has been shown to converge to a piecewise-constant solution, i.e. a solution that has zero gradient at most locations and a limited number of locations with high gradient magnitude. Shock formation at edges and smoothing of details at other locations is the mechanism by which the solution is achieved. The parameter μ controls the degree of edge preservation; however, it is not a simple threshold. Points with gradient magnitudes less than μ may form shocks and be incorporated into edges in the presence of many points with strong gradients nearby. On the other hand, isolated points with large gradient magnitudes will be smoothed. Motivated by this successful method, one approach to smoothing a height map is to treat it as an intensity image and apply P&M anisotropic diffusion directly.

Figure 2(c) illustrates the problems with this approach; P&M anisotropic diffusion causes a "staircasing" effect. This effect has been documented in [25, 19] and is caused by shocks forming at seemingly random locations in regions of high, uniform gradient magnitude, e.g. the slopes of a mountain in terrain data.

4 Feature preserving smoothing for height maps

The original P&M anisotropic diffusion fails when applied to terrain data as shown in Figure 2(c), because it was designed to preserve and create C^0 discontinuities in intensity images to detect edges. However, C^0 discontinuities are very rare in terrain data, they occur only on vertical cliffs. In terrain data, one is instead interested in ridges which are C^1 discontinuities. We would like to find a process that respects C^1 continuous regions such as the slopes of a mountain and preserves and creates C^1 discontinuities.

Let us consider the parametric surface $\mathcal{M}$ defined by the height map

$$\mathcal{M}(x, y) = (x, y, h(x, y)) . \tag{3}$$

The area of this surface over the domain U is computed as

$$A(h) = \int_U \sqrt{1 + \parallel \nabla h(x, y) \parallel^2}\, dx\, dy. \tag{4}$$

The gradient descent PDE on the first variation of this area is $dh/dt = \nabla \cdot (\nabla h / \sqrt{1 + \parallel \nabla h \parallel^2})$, which was used for smoothing $2\frac{1}{2}$D surfaces [23]. This PDE is the MCF for height maps. It has the appearance of being anisotropic due to the division by $\sqrt{1 + \parallel \nabla h \parallel^2}$ before the divergence operation. However, this is not a feature preserving anisotropic process. The rescaling is the projection of the 3D motion onto the image plane which is a result of representing the 3D surface as a 2D graph.

Explicitly preserving C^1 discontinuities requires a penalty term on the second-order structure of surfaces, i.e. curvature. We propose a family of energies that are surface integrals of penalty functions on total curvature, $\kappa^2_{\mathcal{M}}(x, y)$, which is the sum of the squares of the two principal curvatures. Let $G : \Re \to \Re$ be an arbitrary penalty function, then we define the following family of energy functions

$$E(h) = \int_U G(\kappa_{\mathcal{M}}(x, y)) \sqrt{1 + \parallel \nabla h(x, y) \parallel^2}\, dx\, dy. \tag{5}$$

Notice that if $G(\kappa_{\mathcal{M}}) = 1$, this energy reduces to the area of $\mathcal{M}$. We can penalize the integral of total curvature by choosing $G(\kappa_{\mathcal{M}}) = \kappa^2_{\mathcal{M}}$. However, similar to heat flow in image processing, this energy does not preserve discontinuities because the quadratic penalty function does not permit any outliers. Instead, we use the penalty function that gives rise to P&M diffusion in (1), but replace the image gradient magnitude with total curvature:

$$G(\kappa_{\mathcal{M}}) = 1 - e^{-\frac{\kappa^2_{\mathcal{M}}}{\mu^2}}. \tag{6}$$

The parameter μ determines the range of curvatures that are preserved. Figure 2(d) illustrates the results of smoothing the Mt. Hood dataset using this energy definition.

5 A splitting strategy

A direct minimization of the energy defined in (5) requires solving a fourth-order PDE. This is a computationally expensive and unstable task. In this section, we introduce a strategy that splits the solution into a pair of coupled second-order PDEs that can be solved efficiently.

Step 1a: Total curvature from normal vector variations The first step in our splitting strategy is to express total curvature $\kappa^2_{\mathcal{M}}$ in terms of the normal vectors to the parametric surface $\mathcal{M}$. The normal vector to $\mathcal{M}$ can be found as

$$\mathbf{N} = \frac{1}{\sqrt{1 + h_x^2 + h_y^2}} \begin{pmatrix} h_x \\ h_y \\ -1 \end{pmatrix}, \tag{7}$$

where h_x and h_y denote the *x* and *y* partial derivatives of the height map h. Lets define the 3×2 matrix of the gradient of the normal vectors in the image plane

$$\nabla \mathbf{N} = \begin{pmatrix} \mathbf{N}_x , & \mathbf{N}_y \end{pmatrix}. \tag{8}$$

Also define the 2×3 matrix that projects $\nabla \mathbf{N}$ into 3D space

$$\mathbf{P} = \frac{1}{\left(1 + h_x^2 + h_y^2\right)^{3/2}} \begin{pmatrix} 1 + h_y^2 & -h_x h_y & h_x \\ -h_x h_y & 1 + h_x^2 & h_y \end{pmatrix}. \tag{9}$$

The variation of the normal vectors intrinsic to the height map surface is $\nabla_h \mathbf{N} = \nabla \mathbf{N} \mathbf{P}$. Then total curvature can be found as

$$\kappa^2_{\mathcal{M}} = \parallel \nabla_h \mathbf{N} \parallel^2, \tag{10}$$

where the norm denotes the *Frobenius norm* of the 3×3 matrix, which is the square root of the sum of the squares of all of the matrix elements.

Step 1b: Decoupling the normals from the height map The second step in our strategy is to decouple the normal vectors from the surface defined by the height map. Substituting (10) in (5) gives

$$E(\mathbf{N}) = \int_U G\left(\parallel \nabla_h \mathbf{N} \parallel\right) a(x, y)\, dx\, dy, \tag{11}$$

where $a(x, y) = \sqrt{1 + \parallel \nabla h(x, y) \parallel^2}$. We initialize the normal vectors according to (7). Then we fix h and process the normal vectors to minimize the energy (11). Since normal vectors have to remain unit length, this is a constrained minimization problem, which is accomplished by the following second-order PDE on the normal vectors:

$$\frac{\partial \mathbf{N}}{\partial t} = -\left(\mathbf{I} - \mathbf{N} \otimes \mathbf{N}\right) \nabla \cdot \left(a(x, y)\, G'\left(\parallel \nabla_h \mathbf{N} \parallel\right) \nabla_h \mathbf{N}\right), \tag{12}$$

where $\otimes$ denotes the tensor product, and G' is the derivative of G. The operator $\mathbf{I} - \mathbf{N} \otimes \mathbf{N}$ projects the change vector to

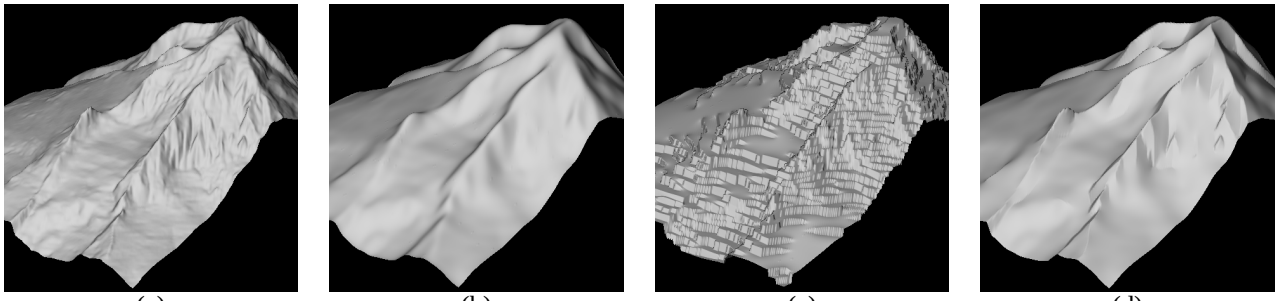

(a) (b) (c) (d)

Figure 2: (a) A portion of the $2\frac{1}{2}$D surface defined by the Mt. Hood DEM, (b) Gaussian smoothing of the height image, (c) P&M diffusion on the height image, and (d) our generalization of P&M diffusion to $2\frac{1}{2}$D surfaces.

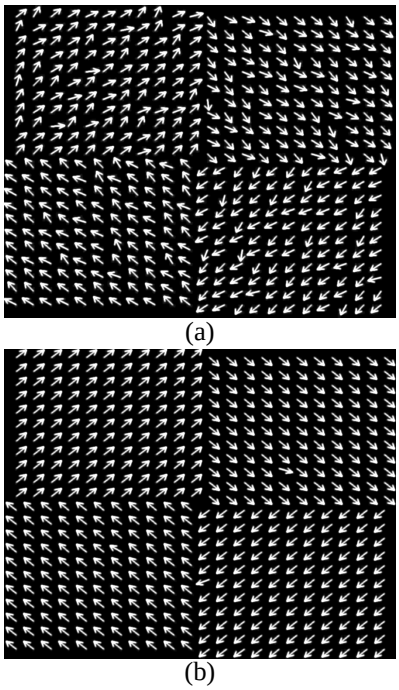

(a) (b)

Figure 3: (a) An image of noisy unit vectors, and (b) the result of minimizing the robust curvature energy.

$\mathbf{N}$ onto the plane perpendicular to $\mathbf{N}$, thus enforcing that the normal vectors remain unit length.

This PDE is the generalization of P&M anisotropic diffusion for a field of unit vectors defined on a $2\frac{1}{2}$ surface. Figure 3(a) illustrates an artificial image of noisy unit length vectors. The vectors were chosen to have a different mean each quadrant of the image. Figure 3(b) illustrates the results of smoothing this vector image with the PDE (12) and with G as defined in (6). The discontinuities in the normals between the quadrants are preserved while the noise within the quadrants is smoothed.

Step 2: Refitting the height map to the normal vectors
Since our goal is to denoise the height map, we have to relate the processing of the normal vectors back to the surface. We do this with a refitting step that minimizes an energy that reflects the discrepancy between the height map surface and

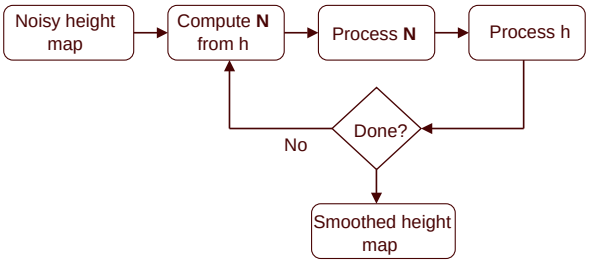

Figure 4: Flow chart.

the processed normal vectors. This energy is

$$D(h) = \int_U \mathbf{N}_h \cdot \mathbf{N}_h - \mathbf{N}_h \cdot \mathbf{N}_p \, dx \, dy, \qquad (13)$$

where $\mathbf{N}_h$ and $\mathbf{N}_p$ denote the normal vectors computed from h according to (7) and the processed normal vectors obtained from iterating the PDE (12), respectively. Let $\mathbf{N}_p = \begin{pmatrix} n_1 & n_2 & n_3 \end{pmatrix}^T$, then

$$D(h) = \int_U \sqrt{1 + \| \nabla h \|^2} - \nabla h \cdot \begin{pmatrix} n_1 \\ n_2 \end{pmatrix} + n_3 \, dx \, dy. \qquad (14)$$

The gradient descent for the first variation of this energy with respect to h is

$$\frac{dh}{dt} = -\nabla \cdot \left(\frac{\nabla h}{\sqrt{1 + \| \nabla h \|^2}} - \begin{pmatrix} n_1 \\ n_2 \end{pmatrix} \right). \qquad (15)$$

5.1 The algorithm

The flow chart for the algorithm is shown in Figure 4. The normals processing stage of the algorithm computes the gradient descent for the normals (12) for a fixed number of iterations (25 for the experiments in this paper). Hence, we avoid evolving evolving the normals too far away from their initialization from h. The height map fitting to the processed normal vectors is given as a gradient descent PDE in (15). This stage of the algorithm is run until the discrepancy measure (13) between the new normals and the normals of the

height map ceases to decrease, which signals the need for another round of processing the normal vectors. The overall algorithm repeats these two steps to denoise the input height map. This algorithm consists of solving two second-order PDEs in series instead of a direct fourth-order PDE, which makes it computationally tractable.

5.2 The parameters

There are two free parameters in our algorithm: μ and the number of iterations of the main loop in Figure 4. The conductance parameter μ determines the range of curvatures that is smoothed and the range that is preserved. As in P&M image diffusion, it is not a simple threshold. In was fixed at 0.1 for all of the results shown in this paper. Unlike, in P&M image diffusion, this parameter does not need to be changed for different surface models. In the context of P&M image diffusion, the units of μ are in gray levels; consequently, the optimal choice of μ is image dependent. However, for surfaces, the units are in curvature, which is data independent. This makes it possible to choose a μ value that gives consistent results over a broad range of surfaces.

The number of times we repeat the main loop (processing the normal vectors followed by refitting) determines the amount of smoothing applied to the data. This is the second free parameter in the system. In Section 6, we present experimental results that illustrate various amounts of smoothing. This parameter could be exchanged for a data term weight by posing the smoothing problem as a reconstruction problem. In a reconstruction problem the energy will be a weighted sum of a smoothness term and a data term. A PDE that minimizes this type of energy is run until convergence, and the free parameter is the relative weighting between the two terms.

6 Experiments

In this section, we present experiments with two different DEM datasets. We demonstrate the effectiveness of our approach as a pre-processing step for ridge/gully detection. There are multiple definitions of a ridge. For terrain data, we consider a ridge to be points of local maximum curvature on the isocurves of the height function $h(x, y)$. The curvature of the isocurves of $h(x, y)$ can be found as

$$\kappa = \frac{h_y^2 h_{xx} - 2h_x h_y h_{xy} + h_x^2 h_{yy}}{\left(h_x^2 + h_y^2\right)^{3/2}}. \qquad (16)$$

Let $\mathbf{T}$ be the tangent vector to the isocurves of $h(x, y)$. Then point of maximal curvature of the isocurves are found as the zero crossings of the following directional derivative:

$$\frac{d\kappa}{d\mathbf{T}} = 0. \qquad (17)$$

Among points that satisfy this equation, those with $\kappa > 0$ are ridges and those with $\kappa < 0$ are gullies.

The main point of this discussion is not the ridge detection itself, but the role of our smoothing algorithm as a preprocessing step. Equation (17) involves third derivatives of $h(x, y)$; therefore, it is hard to compute stably. Typically, these third derivatives of Gaussian kernels are used for this computation. However, the Gaussian kernels eliminates and dislocates ridge lines. We propose that like P&M diffusion is a better choice than Gaussian smoothing for edge detection in intensity images, our anisotropic smoothing algorithm is a better approach for smoothing the data for purposes of ridge/gully detection.

Figure 5(a) illustrates the surface defined by the original 1024×1024 Mt. Hood height data. Figure 5(b) and (c) illustrate the results of smoothing with the proposed approach after 2 and 10 iterations of our algorithm, respectively. One iteration takes approximately 20 minutes for this data set on a *Intel 1.7 Ghz* processor. For denoising purposes a couple of iterations are sufficient. More iterations start forcing the surface towards being piecewise planar. The prominent structure of the mountain is preserved as the smaller scale detail and noise is eliminated. This can be performed as preprocessing for ridge detection or compression.

Figure 6 illustrates the ridge/gully detection experiment. The blue and the red curves on the surface depict ridges and gullies, respectively. For the results shown in the top row, we used a Gaussian smoothing kernel with a low and a high standard deviation. The low standard deviation did not denoise the data enough; hence, there are a lot of false positives in the detection results. On the other hand, the high standard deviation Gaussian resulted in too many false negatives, i.e. missed ridges. Figures 6(c) and (d) illustrate detection results obtained by using the proposed anisotropic diffusion as the smoothing step (after 10 and 20 iterations, respectively). The results are much better than with Gaussian smoothing. For instance, the prominent ridge running down the center right side of the mountain was missed in both low and high standard deviation Gaussian smoothing results. In contrast, this ridge was able to self-organize and strengthen during anisotropic diffusion and was successfully detected. In summary, the detection results with anisotropic diffusion have fewer false positives **and** fewer false negatives.

Figure 7 illustrates a different type of terrain: the transition from a flat valley to rolling hills. Two shallow river beds can be observed as depressions in the valley. Figure 7 (a) shows the original height surface, while (b) and (c) show the surface after 1 and 10 iterations of our algorithm. Figures 7(d)-(f) illustrate the corresponding detection results. Although, only a minimal amount of smoothing can be observed in Figure 7(b), the corresponding detection result shown in Figure 7(e) is much better than the detection from the original data in Figure 7(d). Notice that both of the shallow river beds were detected as gullies. Further anisotropic smoothing results in a cleaner detection, but also losses the weaker river bed. The processing times for this smaller data set was approximately 3 minutes per iteration on a *Intel 1.7 Ghz* processor.

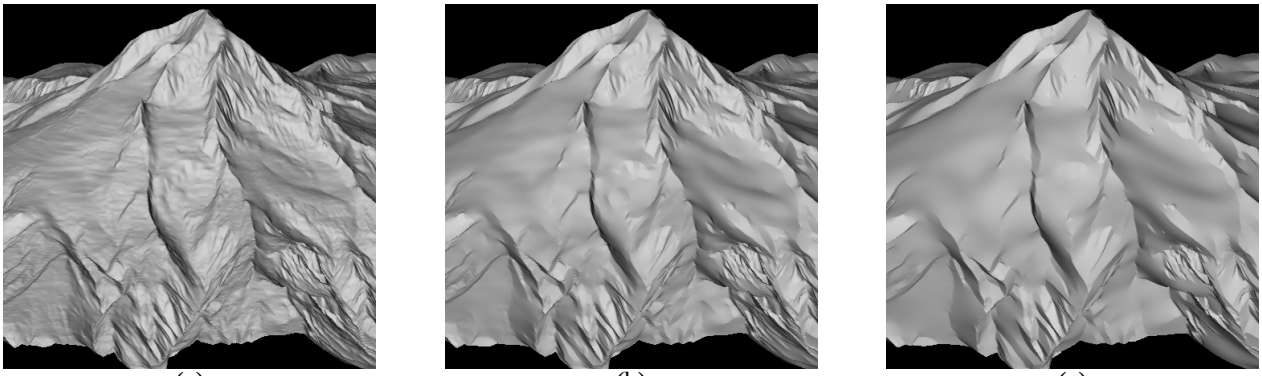

(a) (b) (c)

Figure 5: (a) Mt. Hood, (b) after 2 iterations, and (c) 10 iterations of the main processing loop.

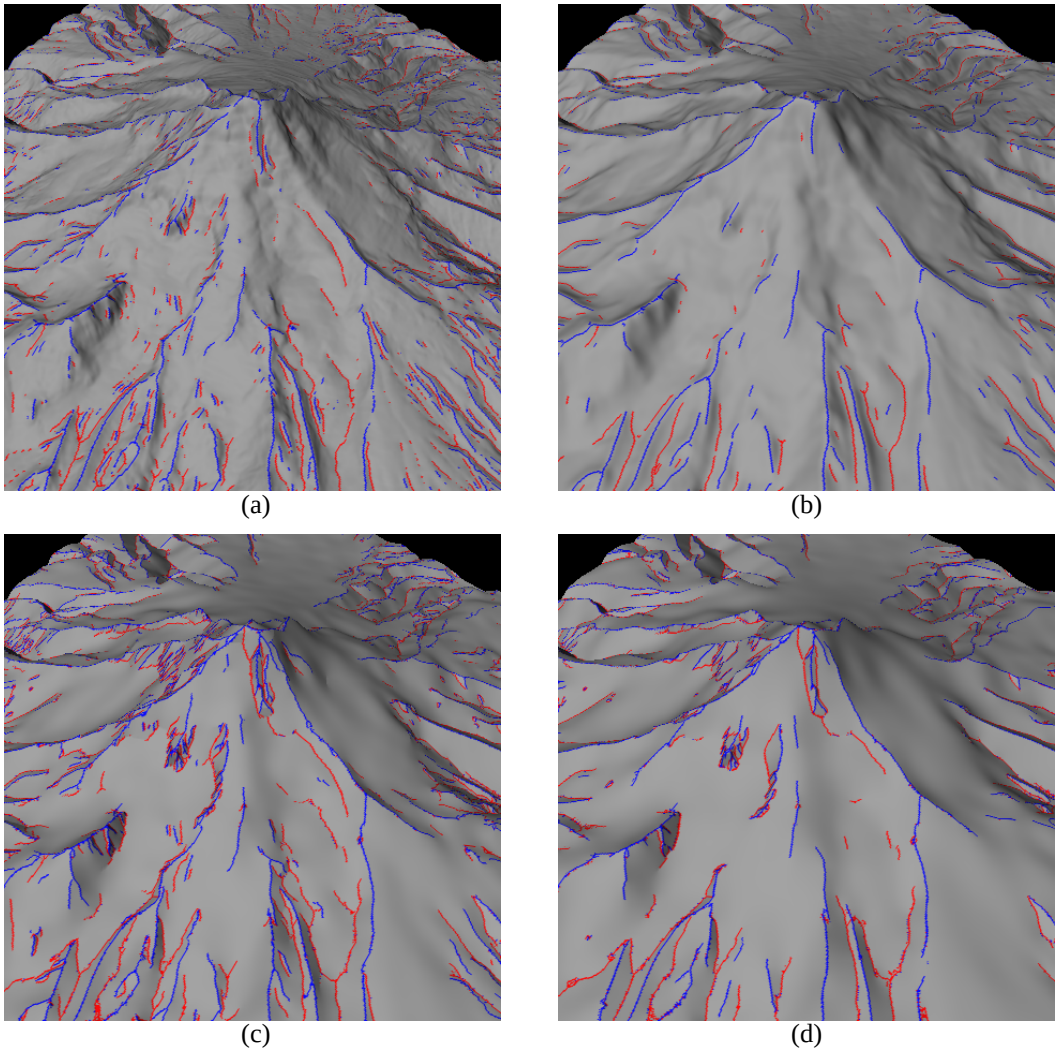

(a) (b) (c) (d)

Figure 6: Ridge and gullies are depicted by blue and red curves, respectively. Results using Gaussian kernels with standard deviation (a) 1 pixel and (b) 3 pixels. Results using our anisotropic smoothing with (c) 10 iterations, and (d) 20 iterations.

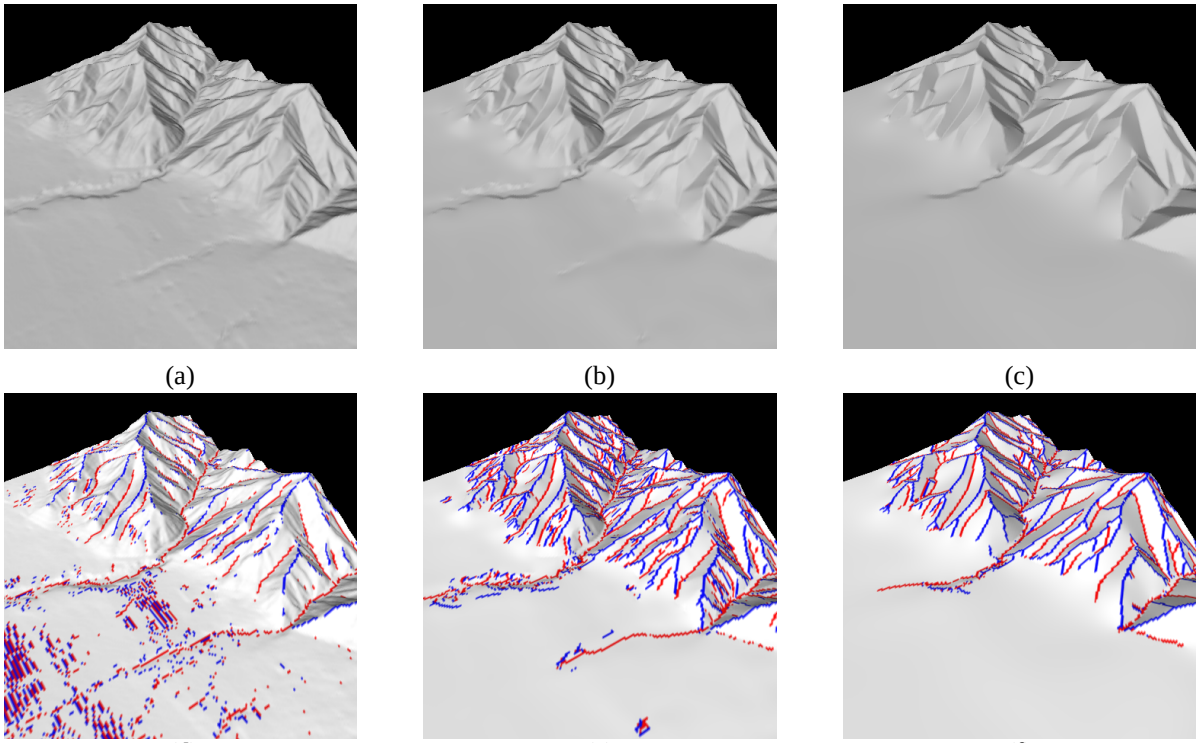

Figure 7: (a) Original data, (b) after 1 iterations, and (c) 10 iterations of our algorithm. Ridges (blue) and gullies (red) detected from the respective data sets on the first row.

7 Conclusions

We derive a variational generalization of P&M anisotropic diffusion for feature preserving smoothing of terrain data. The proposed method is derived from the geometry of $2\frac{1}{2}$D surfaces. It preserves and enhances discontinuities in the surface normal vectors; hence, forcing surfaces towards piecewise smoothness. This type of processing is better suited to terrain data than direct applications of image processing techniques and their heuristic modifications.

Measures on surface normal variations require solving fourth-order PDEs on level sets. However, by processing the normals separately from the surface, we can solve a pair of second-order equations instead of a fourth-order equation. This method is numerically more stable and computationally less expensive than solving the fourth-order PDE directly. The shortcoming of this method is the computation time; however, the process lends itself to parallelism, and therefore, the use of multi-threading. Also, recent developments in solving nonlinear image PDE on commodity graphics hardware promise significant speed-ups for our algorithm [15].

Acknowledgements

This work is supported in part by ONR (#N00014-01-10033), NSF (#CCR0092065) and ARO (DAAD19-01-1-0013).

References

[1] M. J. Black, G. Sapiro, and D. H. Marimont. Robust anisotropic diffusion. *IEEE Transactions on Image Processing*, 7(3):421–432, March 1998.

[2] A. Blake and A. Zisserman. *Visual Reconstruction.* MIT Press, 1987.

[3] U. Clarenz, U. Diewald, and M. Rumpf. Anisotropic geometric diffusion in surface processing. In *Proceedings of IEEE Visualization*, pages 397–405, 2000.

[4] M. Desbrun, M. Meyer, M. Schroder, and A. Barr. Implicit fairing of irregular meshes using diffusion and curvature flow. In *Proceedings of SIGGRAPH'99*, pages 317–324, 1999.

[5] M. Desbrun, M. Meyer, P. Schroder, and A. H. Barr. Anisotropic feature-preserving denoising of height fields and bivariate data. In *Graphics Interface*, 2000.

[6] W. E. L. Grimson. *From images to surfaces: A comp. study of the human early vision system.* MIT Press, 1981.

[7] I. Guskov, W. Sweldens, and P. Schroder. Multiresolution signal processing for meshes. In *Proceedings of SIGGRAPH'99*, pages 325–334, 1999.

[8] M. Halstead, M. Kass, and T. DeRose. Efficient, fair interpolation using catmull-clark surface. In *Proceedings of SIGGRAPH'93*, pages 35–44, 1993.

[9] Ravikanth Malladi, James A. Sethian, and Baba C. Vemuri. Shape modeling with front propagation: A level set approach. *IEEE Trans. on PAMI*, 17(2):158–175, 1995.

[10] H. P. Moreton and C. H. Sequin. Functional optimization for fair surface design. In *Proceedings of SIGGRAPH'92*, pages 167–176, 1992.

[11] N. Nordstrom. Biased anisotropic diffusion—a unified regularization and diffusion approach to edge detection. *Image and Vision Comp.*, 8(4):318–327, 1990.

[12] P. Perona and J. Malik. Scale space and edge detection using anisotropic diffusion. *IEEE Trans. on Pattern Analysis and Machine Intelligence*, 12(7):629–639, July 1990.

[13] T. Preuer and M. Rumpf. A level set method for anisotropic geometric diffusion in 3d image processing. *SIAM J. Appl. Math.*, 62(5):1772–1793, 2002.

[14] L. Rudin, S. Osher, and C. Fatemi. Nonlinear total variation based noise removal algorithms. *Physica D*, 60:259–268, 1992.

[15] M. Rumpf and R. Strzodka. Nonlinear diffusion in graphics hardware. In *Proceedings of EG/IEEE TCVG Symposium on Visualization VisSym '01*, pages 75–84. Springer, 2001.

[16] T. Tasdizen, R. Whitaker, P. Burchard, and S. Osher. Geometric surface smoothing via anisotropic diffusion of normals. In *IEEE Visualization Proceedings*, pages 125–132, 2002.

[17] G. Taubin. A signal processing approach to fair surface design. In *Proceedings of SIGGRAPH'95*, pages 351–358, 1995.

[18] D. Terzopoulos. *Multiresolution Computation of Visible-Surface Representations.* PhD thesis, MIT, 1987.

[19] J. Tumblin and G. Turk. Lcis: A boundary hierarchy for detail-preserving contrast reduction. In *SIGGRAPH'98 Conference Proceedings*, pages 83–90, 1999.

[20] U.S. Geological Survey. http://www.usgs.gov. 807 National Center, Reston, VA 20192, USA.

[21] Jeffrey P. Walker and Garry R. Willgoose. On the effect of digital elevation model accuracy on hydrology and geomorphology. *Water Resources Research*, 35(7):2259–2268, 1999.

[22] W. Welch and A. Witkin. Free-form shape design using triangulated surfaces. In *Proceedings of SIGGRAPH'94*, pages 247–256, 1994.

[23] R. Whitaker. On the reconstruction of height functions and terrain maps from dense 3D data. In *IEEE International Conference on Image Processing*, 2001.

[24] Ross T. Whitaker. A level-set approach to 3D reconstruction from range data. *Int. J. Computer Vision*, 29(3):203–231, 1998.

[25] Ross T. Whitaker and Stephen M. Pizer. A multi-scale approach to nonuniform diffusion. *Computer Vision, Graphics, and Image Processing: Image Understanding*, 57(1):99–110, January 1993.